
Article:
Desai, P.D. and Zimmerman, W.B. orcid.org/0000-0001-7123-737X (2023) Transient effects and the role of wetting in microbubble generation. Current Opinion in Colloid & Interface Science, 67. 101722. ISSN: 1359-0294

https://doi.org/10.1016/j.cocis.2023.101722

Available online at www.sciencedirect.com

ScienceDirect

Current Opinion in
Colloid & Interface Science

Transient effects and the role of wetting in microbubble generation

Pratik D. Desai[1,2] and William B. Zimmerman[1]

Abstract

Microbubble dispersions are now commonly deployed in industrial applications ranging from bioprocesses to chemical reaction engineering, at full scale. There are five major classes of microbubble generation devices that are scalable. In recent years, some of these approaches have been explicitly studied for the influence of wetting properties on microbubble performance, for which the major proxy is the bubble-size distribution. In this piece, the methodologies for inferring bubble-size distribution are explored, with several recent advances as well as their potential pitfalls. Subsequently, studies where microbubble generation has been under investigation for wetting effects are assessed and in some cases, those that were not allowed the deduction that wetting is a significant factor. Two particular studies are highlighted: (i) systematic variation of wetting effects within a venturi with removable walls substituted with coated walls of known contact angle with hydrodynamic cavitation induced microbubbles and (ii) variation of ionic liquids with staged fluidic oscillation before steady flow. The first study shows that even in scenarios where high inertial effects would be expected to dominate, wetting influences are significant. The second study shows that transient effects are strongly influenced by both imbibition into pores and surface wetting but that viscous resistance is always a key factor. From the exploration of these recent studies, specific recommendations are made about how to assess the influence of wetting in those mechanisms/devices where it has not been explicitly studied, via deduction from those mechanisms/devices where the effects are demonstrably significant and indeed in some cases, controlling. In study (ii), which is the first to blow micro/bubbles into ionic liquids, wetting and transient effects are reasonable for between 25% and 50% reduction in average bubble size, although up to 70% reduction is observable when viscous effects are dominant, relative to the control of steady flow with the same pressure drop. Indeed, staging transient operations shows both bubble-size reduction and increased volumetric throughput are simultaneously possible.

Addresses

[1] Department of Chemical and Biological Engineering, Mappin Street, University of Sheffield, Sheffield, S1 3JD, United Kingdom
[2] Perlemax Ltd., 318 Broad Lane, S3 7HQ, Sheffield, United Kingdom

Corresponding author: Zimmerman, William B. (w.zimmerman@sheffield.ac.uk)

Current Opinion in Colloid & Interface Science 2023, **67**:101722

This review comes from a themed issue on **Wetting and Spreading (2023)**

Edited by **Tatiana Gambaryan-Roisman** and **Victor Starov**

For complete overview about the section, refer Wetting and Spreading (2023)

https://doi.org/10.1016/j.cocis.2023.101722

Keywords

Microbubbles, Bubble size distribution, Wetting effects.

Introduction

The common industrial mechanisms for generation of submerged microbubbles where gas is inserted into liquid are classified into flow through microporous diffusers (Wesley et al., 2016), saturation-nucleation as implemented for dissolved air flotation [1], Venturi effect through nozzles Fujiwara et al. [2], hydrodynamic cavitation [3], and rotary gas−liquid flow [4,72]. Among these, the Venturi nozzle approach entrains air before dispersing it as bubbles. The other approaches inject air, but of course for the Venturi nozzles, injecting liquid likely requires high power consumption to achieve similar gas-phase bubble fluxes. Hydrodynamic cavitation is often the result of fluidic devices that inject liquid. For a net gas-phase bubble flux, if the liquid has no dissolved gases, the cavitation bubble that is formed consists of the vapour of the liquid. Surfactants in the liquid can stabilize the gas−liquid interface of the microbubble (see [5]), so that mass transfer is effectively blocked. The inference from Figure 6 of Krazn et al. [6] is that in surfactant-laden solutions, 1.3- to1.5-mm diameter bubbles achieve equilibrium absorption on the order of a few hundredths of a second, providing a strong stabilization mechanism exploited in biomedical applications for imaging [7] and drug delivery [8]. However, if the carrier gas is important, saturated or supersaturated liquid results in cavitation microbubbles that require no surfactant stabilization.

As there are three phases involved, the fact whether the liquid wets the solid walls of the injection system could play a critical role in the resulting bubble-size distribution (BSD), relative to the orifice-length scale used for injection and, in general, the formulation dynamics. The gas and liquid flow rates, as well as transient profiling of these flow rates, might also influence the

normalized BSD and the accompanying formulation dynamics. The purpose of this paper is to analyse the recent literature concerning these central questions of wetting, gas and liquid flow rates, and transient effects on the aforementioned categories of microbubble-injection approaches.

The initial point of departure is Wesley et al. (2016). Those authors considered disperse air injection with specially prepared microporous diffusers so that the contact angle is tuneable by deposition of a coating. Wetting is demonstrated to change dramatically the normalized BSD with a bifurcation to much larger average bubble sizes with critical contact angle $\theta = 90°$. With decreasing liquid wetting and $\theta < 90°$, the normalized average bubble size increases. However, with decreasing liquid wetting and $\theta > 90°$, the normalized average bubble size jumps at the critical contact angle substantially as conjunctions of bubbles emanating from neighbouring pores form more readily, with the resultant bubble having the combined volume of the progenitor bubbles. Hence, wetting effects are substantially controlling with steady-state flow through microporous diffusers.

The paper is organized as follows. Section Microbubble size inference methods reviews the methods of bubble-size characterisation. Section Wetting influences with various microbubble generation methods reviews the literature concerning wetting influences in microbubble generation from the mechanisms for gas insertion into liquids via microbubbles. Section Discussion and Conclusions contains discussion of the learning from this analysis of the literature and draws conclusions.

Microbubble size inference methods

The quality of an injection method for microbubbles is assessed largely through the BSD, which is an extensive measure from which the bubble-phase volume fraction in the liquid can be computed. Some applications require a narrow distribution around a target-size range, such as flotation, where bubbles near the size of the target particles to be floated increase performance dramatically [9]. Many applications controlled by transport phenomena have been modelled traditionally as only dependent on the surface area of bubble-phase dispersed in the liquid [5], so a wide size distribution would be considered acceptable. Superficially, then, the influence of wetting and transient effects in microbubble formation should be assessed from the BSD and associated liquid- and gas-phase flows used to achieve it.

There are essentially two overarching classifications of bubble-size analysis approaches—optical and pressure wave methods—but with several categories within each. §2.1 explores the optical methods, while §2.2 scrutinizes the sound-wave methods.

Optical approaches to inferencing BSD

Direct image analysis

Desai et al. [10] reviews the commonly adopted approach, since Wesley [11], of automating the image capture and analysis using the high-speed, high-precision photography and microscopy, with the analysis conducted using common computational toolboxes in Octave, ImageJ, MATLAB, Mathematica, or Labview. Many such analyses are in support of an application of microbubbles, with the most common being flotation, as reviewed by Schmideder et al. [12], who also introduce a purpose-built inline microscopy imaging instrument. Typical of these studies that develop *de novo* such a do-it-yourself BSD approach is Le et al. [13], which aims to use dispersed CO_2 microbubbles in aqueous solution for enhanced oil recovery and carbon sequestration.

The recent novel approaches in this category are a commercial microscopy instrument as a submersible probe, the Anglo Platinum Bubble Sizer®, manufactured by Stone Three® in South Africa [14], and image analysis of microscopy with shadowgraphy in low-light conditions [15]. As pointed out by Desai et al. [10], such direct optical methods have two major drawbacks: (i) they must be conducted in a translucent, if not transparent, liquid solution and (ii) as readily observable by scrutiny of adjacent frames, smaller bubbles are occluded by larger bubbles, so they do not get counted. To overcome the latter, the analysis approach would have to treat multiple images and detect smaller bubbles emerging from behind larger bubbles, which would seem insurmountable in a dense microbubble cloud.

Scattering and photonic methods

The use of statistical inversion of multiple Fraunhofer diffraction patterns to infer particle-size distributions was pioneered by Swithenbank et al. [16] at the University of Sheffield, eventually commercialised as the Malvern Mastersizer. In terms of the approach, microbubbles present no differently than small particulates, so the method produces a BSD. Couto et al. [17] are credited with the first use of the Fraunhofer diffraction inference of BSD. A submersible laser-diffraction particle-size analyser called the LISST-200X (Sequoia Scientific Inc.) has been adapted to microbubble BSD estimation using Fraunhofer inferencing [18]. Desai et al. [10] report on the adaptation of the Malvern Spraytec, commonly used for droplet-sizing in sprays in "midair", to microbubble dispersion BSDs in liquids at a time similar to Tesar et al. (2013).

The recent novel approaches in this category are the use of process analytical techniques such as focused beam reflectance measurement (FBRM G400, Mettler Toledo) by Gao et al. [19] and volume scattering function inversion for BSD (Angara et al., 2021), which uses a fuller range of Mie scattering functional analysis than Fraunhofer diffraction.

As with direct optical methods, scattering and photonic methods require translucent or even transparent solutions to be effective, hence densely packed (high void fraction) and "milky white" microbubble dispersions are unapproachable. The more recent deployments are generally noninvasive.

Sound waves: acoustic bubble spectroscopy and ultrasonic transmission analysis

It has long been recognized that bubbles are influenced by sound waves [20] with resonant interactions in the acoustic regime and a range of scattering − diffraction, refraction, and reflection—in either sonic or ultrasonic regimes [21]. Geometrical acoustics underpins sonar technology that is either passive, listening to signatures of bubbles, or active, pinging off surrounding features. Acoustic bubble spectroscopy builds on geometrical acoustics for the reconstruction of the BSD from transmitted and received pure acoustic frequencies. Chahine et al. at Dynaflow have developed a commercial product for characterising microbubble BSD in multiple different scenarios [22−25]. Shin et al. [26] made a novel use to map the wake of a planing hull. More recently, Desai et al. [10, 27] have reported on microbubble cloud BSDs generated by fluidic oscillation of air through microporous diffusers.

The novel entrant in this category exploits *ultrasonic* transmission with several frequencies and Fredholm integral inversion [28]. The algorithm uses a combination of data assimilation from a training set to improve a model that is then trialled on a (micro)bubbly flow for inversion of the transmission and resonance results from a small number of frequencies. Although impressive in its inference accuracy with the semiempirical model, it is uncertain how well the approach generalizes.

Desai et al. [10] conducted a comparison study of the major direct optical, photonic, and acoustic approaches to characterise microbubble clouds generated by fluidic oscillation. The general learning is that hydrophones have to be impedance matched, once submerged, with the acoustic impedance of the liquid medium, which must be estimated as a precondition for acoustic bubble spectroscopy. Spraytec optical paths provide constraints on the material and configuration of vessel construction such as index of refraction. However, both of these inference methods give comparable estimates of BSDs. Nevertheless, there is no simple solution for benchmarking a diagnostic methodology with a known calibration such as Chen et al. [28] that is universally applicable.

Wetting influences with various microbubble generation methods

The quality of an injection method for microbubbles has been shown by Wesley et al. [29] to be dependent on the wetting properties of the solid material by the liquid when gas-contacted as assessed by BSD for the class of dispersed air microbubble generation. This section explores the importance of wetting in recent studies for all classes of microbubble injection methods mentioned in the Introduction.

Saturation−nucleation microbubble generation as used by dissolved air flotation

Often nicknamed the "Coca Cola" mechanism, the saturation-nucleation approach generates gas-saturated liquid at a substantial overpressure, say 3−5 bar, and then releases the saturated liquid through a submerged nozzle into the liquid close to ambient pressure. This approach underpins probably the largest and longest standing microbubble-mediated process—dissolved air flotation (DAF) [9].

The literature concerning DAF and wetting effects almost exclusively focuses on the hydrophobicity of the particulate matter to be floated, and the tuning of the surfactant chemical additives to facilitate bubble−particle attachment. Krasowska et al. [30] studies the thin film stability between bubbles and particles using interferometry, as well as its modification with polymer additives. In general, the modification of particle properties to achieve hydrophobicity and selective flotation, for one plastic from another, for instance, is a common theme reviewed recently by Wang et al [31]. Similar questions arise in minerals engineering [32].

By contrast, the effects of the ionic and/or surfactant content of the liquid media most influence the bubble coalescence mechanism, near or within the nozzle, so are the most likely to be influenced by wettability of the solid by the liquid solution within the nozzle. Unfortunately, there appear no studies on these internal dynamics of wetting. Instead, Liu et al. [33] consider the boundary conditions on the drainage flow in the film between approaching bubbles while exploring mechanisms for bubble coalescence that is influenced by wetting, including ionic strength. Vakarelski et al. [34] study the fundamental dynamics of bubble collisions and the controlling role of interfacial mobility, or its counterpart immobility due to surfactant loading, on bubble coalescence.

Computational fluid dynamics modelling of bubbly flow with population balance equations models have been developed for the contact zone of dissolved air flotation [35,36], with differing modelling approaches characterising BSD and associated dynamics. Both compared their predicted BSDs with those found experimentally from Chen et al. [35]. Yang et al. [36] compared their predicted steady-state flow structures with velocimetry. Good agreement was found to the BSDs, with a modestly better fidelity for the more elaborate bubble-size binning approach by Yang et al. This level of

predictive modelling is impressive for, arguably, the largest volume microbubble unit operation globally. From the prospective of the interest of this review in evaluating the importance of wetting effects, both studies are silent. The wetting effects are likely to be important in the nozzle region where three phase contacts occur, but both modelling approaches treat the inlet condition to the DAF tank from the nozzle as a summary composition with velocities of each phase, rather than considering how the bubbles form and interact with the nozzle solid boundaries.

Venturi effect nozzles

Fujiwara et al. [2] initiated the use of Venturi effect generation of microbubbles. The impetus was a similar arrangement of flow constriction with an adjacent gas inlet duct by Sadatomi et al. [37], where the constriction was caused by a spherical-body midchannel obstructing the flow, with a turbulent wake that mixes the phases. With a venturi, the duct itself is constricted and then expanded, with the perpendicular gas inlet at the constriction. Flow and pressure modifications draw in gas, entraining and mixing the phases with greater turbulence intensity as the flow rate increases. With selection of appropriate geometry and flow rates, the pressure rarefaction induces cavitation bubbles as well.

Lee et al. (2019) study the addition of swirling-flow upstream in inducing more homogeneous mixing as demonstrated in jet flows [38] and mixing flows [39]. Wang et al. [40] compared performance in microbubble size, computing the Sauter mean diameter for both conventional venturi and swirl-venturi microbubble generation with equivalent flow rates. Nevertheless, it is probably more consistent to consider equivalent pressure drops across the apparata, as the swirl generation incurs substantial dissipation. On that basis, the Sauter mean diameter (smaller) and mass transfer coefficient (larger) indicate better performance. However, only two submillimetre data points in the BSDs with a very long tail of 1- to 10-mm diameter bubbles in both cases are reported, which gives little confidence in the approaches creating tuneable, narrow BSDs. Murai et al. [41] found that careful flow-control in the subsonic regime that avoids pressure shock waves induces fragmentation of the larger bubbles generated in conventional venturi nozzles.

Unfortunately, none of the studies of Venturi effect nozzles, exploiting gas entrainment, have considered wetting effects on microbubble generation performance. This lack of attention probably stems from the widespread impression that the dramatic change in pressure forces is the dominant mechanism, and thus, the materials of construction and their coatings have negligible influence. As all metals, stainless steel is hydrophilic, since metallic ions will readily dissolve in a polar solvent, such as water, resulting in a contact angle less than 90°. Nonetheless, the contact angle on polished stainless steel exhibits a time-dependent transition, initially from a hydrophilic state to a relatively hydrophobic state. The static contact angle of a water droplet was monitored on polished stainless steel surfaces every 24 h, and a rapid increase in the contact angle, from 44° to 81°, was found during the first three days. The contact angle reached 98° in 40 days [42].

Clearly wetting variability is important in all gas–liquid flows. The variability of wetting just in one structural material without coatings implies that wetting is significant. Since hydrophobicity tends to maintain the attachment of air jets to the nozzle wall yet also decreases wall shear dissipation over liquid wetting, there are opposing forces to phase interspersal. This complex interplay must influence emergent BSD.

Hydrodynamic cavitation [3] can result from Venturi effect nozzles with sufficiently severe rarefaction. Li et al. [43] demonstrate that considered selection of the geometry to induce low flow resistance also induces hydrodynamic cavitation, consistent with our hypothesis in the previous paragraph that wetting effects influence the flow regime, so could also influence the onset of hydrodynamic cavitation. Simpson and Ranade [44] identify the onset of hydrodynamic cavitation in venturi nozzles via hydrodynamic modelling. Liu et al. [45] demonstrate hydrodynamic cavitation–induced microbubbles within a liquid flow through a Warren-type jet diversion fluidic oscillator (see [46]). The role of wetting with regards to duct walls within the fluidic oscillator is likely to be negligible. Surfactant or ionic strength of the solvent, however, could be crucial to stabilizing the microbubbles so-induced by hydrodynamic cavitation. More on wetting effects in this scenario is presented in §3.4 on hydrodynamic cavitation.

Rotary gas–liquid flow

Figure 1 shows a diagram explaining the operating principle of the Nikuni pump micrbubble generator. Although the high-speed rotary blades create a highly dissipative turbulent flow, the overall power consumption is substantially less than conventional dissolved air flotation. Clearly, since the aqueous solution in the reservoir is recirculated, there is a substantial filtration requirement for any solids laden solution as solids impingent on high-speed blades will cause pitting damage as well as fouling. Swart et al. [47] use the Nikuni pump for recent microplastic particulate separation, with a separate pure-water tank for recirculation and only inject from this tank into the flotation column. For applications where defouling or cleaning of surfaces, for which this device is well-known, a separate clean water reservoir is used without recirculation.

See, for instance, Song Chung et al. [49]. Sheng et al. [50] used microbubbles generated by the Nikuni KTM rotary pump in two different ways in a complex wastewater treatment—aeration and flotation—in stages. But their only concern over wetting properties was that of tuning flotation.

One would think that gas–liquid–solid wetting properties would be an issue with the rotary blades as the two fluid phases are mixed. As discussed in §3.2, steels are generally hydrophilic but have adjustable properties from the specific allow and can, of course, be coated. There is little information on the material construction of the blades in the Nikuni pump in the open literature. From experience, however, with operating bioreactors [51], unless the steel surfaces exposed to microbubble flows are treated appropriately, they rapidly corrode from the highly aerated water and salts/impurities present, which accelerate this corrosion.

Although there are no explicit studies concerned with wetting influences with rotary pump microbubble performance, inference can be drawn by contrasting two recent studies. Swart et al. [52] developed an automated BSD inference system by image analysis, using the Nikuni rotary pump microbubble generator, demonstrating a mean bubble size of ∼90 microns in water. By contrast, Alfarraj et al. [53] applied similar methods to infer mean bubble size generated in diesel of 6 μm. Although certainly water and diesel have different viscosity and density, it is also true that metallic surfaces that are hydrophilic tend to be oleophobic, which allows that the fluid layer nearest to the blades would be air with mixing of diesel and air in a Nikuni KTM rotary pump microbubble generator. Although the contrast of these two studies does not definitively lead to the conclusion that wetting is the dominant mechanism in rotary pump microbubble generation, it gives sufficient supporting evidence to warrant exploring the use of liquid nonwetting coatings or materials to the blades.

Hydrodynamic cavitation

There are many fluid mechanical devices that can induce hydrodynamic cavitation. Age old wisdom for pump design is avoidance of cavitation for the structural longevity of the mechanics. We have already reviewed two recent advances for platforms to control hydrodynamic cavitation in §3.2, but are there configurations to suggest surface wetting might be an important feature? With ultrasonic cavitation, the position of the cavitation-induced bubbles depends on the rarefaction extrema points from the standing ultrasound wave [54], hence far from solid structures. With hydrodynamic cavitation within say venturis [43,44] or fluidic oscillators [45], the focal point for rarefaction is influenced by the nontrivial geometry of solid walls and by transient effects. So there is the possibility that microbubbles formed by such hydrodynamic cavitation could be near walls and thus influenced by surface wettability. Furthermore, the nucleation could be heterogeneous, which would be influenced by wall structures that are also components of wettability.

Fortunately, into this speculative space, there is the recent study of Li et al. [55]. These authors were looking towards the generation of microbubbles by heterogeneous nucleation on particles with applications in minerals engineering targeted. But they also explored the analogous wettability issues within venturis. The key finding is that venturi tubes of different surface properties showed that the wall surface behaves similarly as particles with regards to microbubble nucleation. Hydrodynamic cavitation was promoted by a more hydrophobic venturi tube, which dominated over the effect of particle-surface properties. The key factor measured is the onset of cavitation via inception velocity through the throat of the venturi. With pregassed deionized water, this factor is roughly independent of contact angle of the solid walls of the throat. With ungassed deionized water, the onset of cavitation is at much lower inception velocities with increasing contact angle—approximately one third decrease from 9° to 74° contact angles, with coated glass tubes.

The study of hydrodynamic cavitation within a self-excited fluidic oscillator by Liu et al. [45] focuses on the transient cavitation number effects, as the pressure

Figure 1

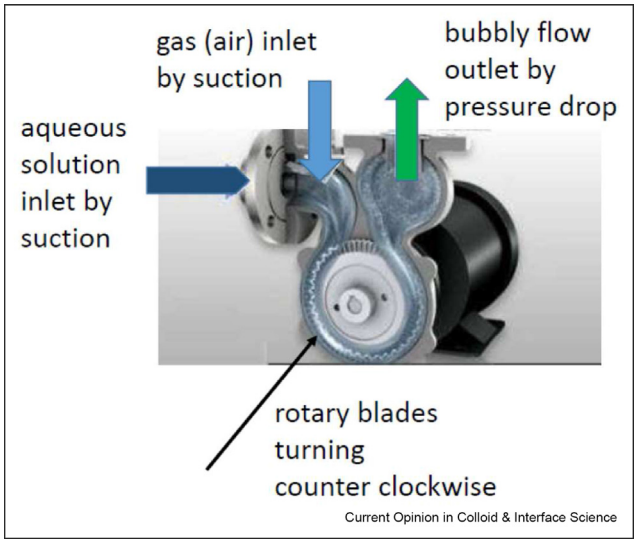

The Nikuni KTM rotary pump microbubble generator operates on the principles described by Li and Tsuge [48]. The high-speed rotary blades draw aqueous solution from the reservoir and gas (air) from the ambient to create a bubbly flow with a narrow size distribution in the low-micron bubble-size regime. Typically, the bubbly flow is recycled to the reservoir.

wave within the main chamber depends on the jet entry velocity and the length of the feedback arms, influencing the oscillation frequency. As the jet entry velocity increases, the region of high cavitation intensity migrates downstream within the chamber. Due to the Coanda effect, this region is always the near one or the other side walls [46].

Microbubbles injected through microporous diffusers

Blowing gas through microporous diffusers induces microbubbles as evidenced by Desai et al. [10], with both steady and fluidic oscillated flow through a microporous alumina—silica ceramic diffuser, commonly used by the aquaculture sector (Point Four MBD75, Pentair), used as an exemplar. With steady flow, the average bubble size is between 350 and 450 μm for a range of throughput velocities. With tuning of the oscillation frequency, 7- to 10-μm average bubble size is noted. This resonant effect stems from generating wavelengths of similar length to the pore diameter. However, substantially larger mean bubble sizes are observed from microporous-sintered alumina ceramic diffusers (HP Technical Ceramics, Sheffield) with fluidic oscillation [56], but without applying resonant methods and with reduced ability to measure gamut of bubble sizes. Nonetheless, the steady flow through each type of diffuser shows that the microporous-sintered alumina ceramic diffuser creates smaller bubbles on average. Song et al. [57] confirm the observation that oscillatory flow through microporous diffusers achieves smaller bubble sizes with liquid wetting.

The major distinction between the diffusers is wettability. Alumina is hydrophobic. Alumina silica is hydrophilic. Tesař [58] showed that fluidic oscillation—generated microbubbles have flow reversal with hydrophilic diffusers during part of the oscillation period, which results in the imbibition of water into the pore and aids the pinch-off of the microbubble at a size smaller than that of steady flow. With hydrophobic diffusers, this effect is much less pronounced. Wesley et al. [11] explored the generation of microbubbles through microporous diffusers with steady flow and systematically varied contact angle via surface coatings. They found that the most dramatic shift in bubble size occurred at critical contact angle $\theta = 90°$. The inference is that liquid-wetting contact angles are best for both steady and oscillatory flows, with the latter, including flow reversal, preferred. Xie et al. [59] showed this liquid wettability trend holds with organic solvents.

There are, however, different notions of "performance" whereby nonwetting surfaces could be preferred. With nonwetting surfaces, the friction along the wall of the pore is largely that of the gas, so that pressure drop is decreased with the same volumetric throughput. With flow reversal and liquid imbibed into the pore [58], there is substantial resistance as the final region of the pore has liquid friction along the pore wall. This increases pressure drop for the same volumetric flow rate. Ideally, one would prefer a decreased average bubble size for greater interfacially mediated phenomena but a lower friction cost and higher volumetric throughput. Is there an approach between steady flow and steady oscillation that could achieve both of these desirable performances?

Desai [60] proposes the hypothesis that a transient flow that is neither steady flow nor steady oscillation, but rather intermediate stages of both, can achieve both smaller average bubble size than steady flow alone, and smaller pressure drop than steady oscillation alone. Rather than water or diesel, the test fluids are room-temperature ionic liquids (RTILs or ILs). The serendipitous observations were part of a larger study of IL and bubble transport phenomena. The test and visualization cell used to explore this transient staging hypothesis has also featured in Taylor et al. [61].

Air is supplied from a pressurised compressed source at 8 bar (g) and moderated downstream by a pressure regulator down to the bubbling pressure required for the target volumetric flowrate.

The systemic pressure is controlled using a pressure regulator, and the flow is controlled using a mass flow controller followed by a fluidic oscillator (FO) connected to the test cell. The visualisation set up is similar to that in Brittle et al. (2015) and Taylor et al. [61] where the light source and camera are placed opposite each other with the rig in the centre in order to obtain maximum contrast and collect the best images possible. The pressure is maintained so that the system is as close an approximation to closed as reasonably possible. Flow matching is performed using a mass flow controller (Bronkhorst - miniCoriFlow) placed at the outlet. Conventional steady flow is used first to generate bubbles at the fixed flow rate. The backpressure for this sparger and design is 40 mbar(g), and the oscillator is operated at 100—110 mbar(g) bringing total system pressure drop to approximately 150 mbar. There are minor variations as this also depends slightly on the frequency of oscillation in the system. The reader is referred to Desai [60] for a more fulsome description.

Maintaining similar conditions, the FO is then introduced to the system, and the bubbles are sized again. This is then replicated with conventional steady flow. This sequence, FO followed by steady flow, defines the staging effect of the hypothesis. Steady flow alone is the control for comparison purposes of the influence of the active principle of staging oscillation before steady flow for bubble generation.

Figure 2

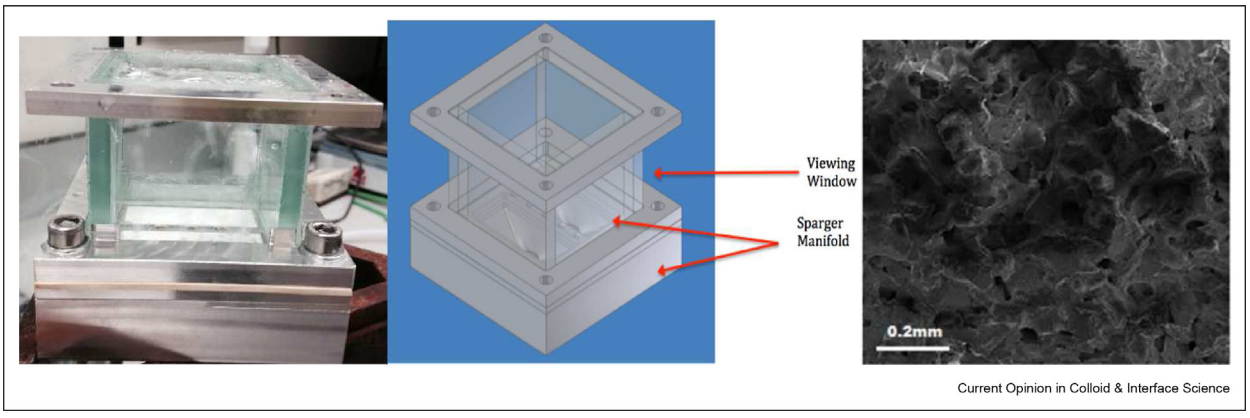

Test Cell (right) and rendering (centre)—with sanning electron microscopy image of the microporous ceramic sparger (right).

ILs used by Desai [60] are selected from those previously synthesised and tested by [61]. 1-Ethyl-3-methylimidazolium dicyanamide [C_2mim][DCA] (98%), 1-ethyl-3-methylimidazolium bis(trifluoromethylsulfonyl)imide [C_2mim][NTf_2] (≥97%), and 1-butyl-3-methylimidazolium bis(trifluoromethylsulfonyl)imide [C_4mim][NTf_2] (≥98%) are used as received from Merck. 1-Ethyl-3-methylimidazolium ethylsulfate ([C_2mim][$EtSO_4$]) is synthesised by dissolving diethylsulfate (Sigma–Aldrich, 98%, 154.2 g, 1 mol) in ice-cold toluene (Sigma–Aldrich, ≥99.5%, 100 cm^3) and adding this solution dropwise to 1-methylimidazole (Sigma–Aldrich, 99%, 82.1 g, 1 mol) dissolved in water (500 cm^3) in an ice bath under a nitrogen atmosphere. This solution is stirred overnight. The organic solvent is then removed, and the former IL is then sequentially washed with toluene (100 cm^3) and dried *in vacuo* five times. 1-Butyl-3-methylimidazolium trifluoroacetate [C_4mim][TFA] is synthesised from trifluoroacetic acid (Sigma–Aldrich, 99%, 114.0 g, 1 mol), added dropwise to 1-butyl-3-methylimidazioum chloride (174.7 g, 1 mol), dissolved in Milli-Q ultrapure water (500 cm^3) in an ice bath, and allowed to stir overnight. The solvent is then removed using a rotary evaporator to obtain the IL. All ILs are dried *in vacuo* ($<10^{-2}$ mbar @ 40 °C) for a minimum of 48 h and are maintained under a flow of dry N_2 overnight before microbubble experiments are conducted. After drying, the water content of the ILs is measured using a Metrohm 787 KF Titrino Karl

Figure 3

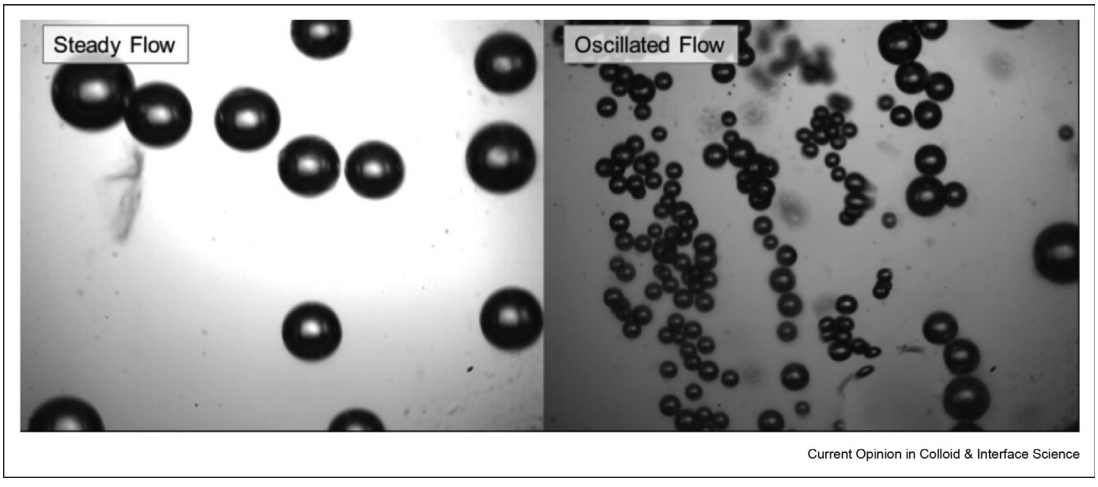

An example of the image captured in the test cell for steady flow (left) and oscillatory flow (right) for a single room-temperature ionic liquid–[C_2mim][DCA]—at equivalent flowrate conditions (50 mL per minute). Scale is 1 mm = 24.56 μm.

Figure 4

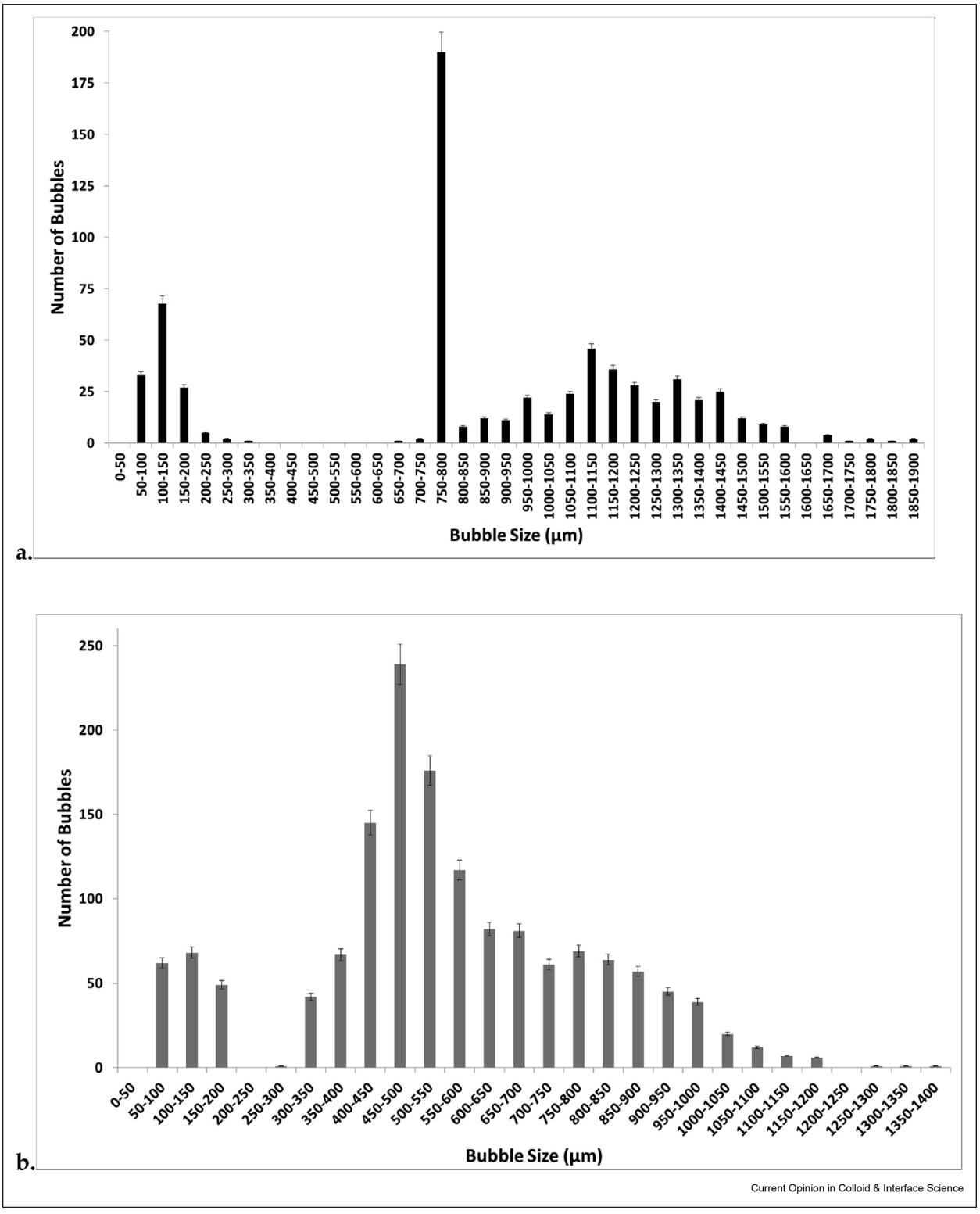

Bubble-size distribution for (**a**) steady flow and (**b**) for fluidic oscillator generated bubbles in [C_4mim] [TFA].

Figure 5

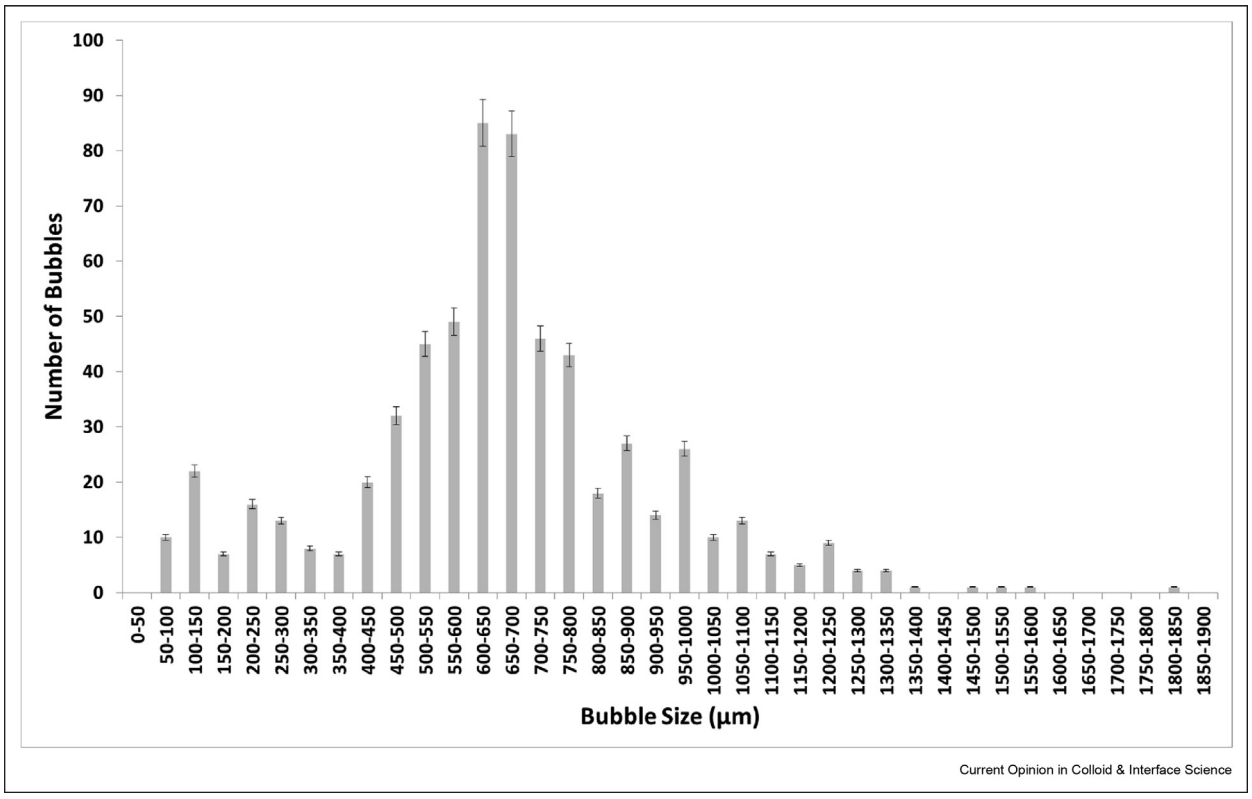

Bubble-size distribution for conventional steady flow post fluidic oscillation (FO) in [C_4mim] [TFA].

Fischer as < 0.1 wt% for all ILs. The purity of the synthesized ILs is analysed using ^{1}H Nuclear Magnetic Resonance using a Bruker 300 MHz Ultra shield Plus Nuclear Magnetic Resonance spectrometer. The resulting physical properties are consistent with prior studies [62,63].

The visualization test cell of Desai [60] is custom-designed for generating bubbles using small samples (50 cm^3—100 cm^3) and with glass windows in order to size the bubbles generated using a high-speed camera. The test cell is designed for low-flow systems with flowrates in millilitres per minute (mLpm) and houses a ceramic multiporous sparger (sparger used—HP Technical Ceramic [fused sintered alumina, 20-µm average pore size, 2 off - '50 × 25' mm^2 area]).

Figure 2 shows the test cell and a scanning electron microscopy (SEM) image of the ceramic sparger used. The visualisation window (quartz windows) allows bubble-size determination by optical imaging. The sparger can be changed in order to collate the best size distribution possible. SEM is carried out on a JEOL JSM 6300 scanning electron microscope with an Agar MB7240 gold sputter coater. This sparger has a thickness of 5 mm, and the pressure required to allow bubbling in an aqueous system is 40 mbar(g) at 298 K and 101.325 kPa.

The contact angle measurements are made using an Attension pendant drop tensiometer for the RTIL. RTILs are kept in a dry environment and are heated to 60 °C for 24 h in order to remove residual moisture whilst maintaining vacuum desiccation in the presence of $CaCl_2$. The Attension pendant drop tensiometer is able to take precise measurements of the contact angle using a visualisation setup similar to the bubble-sizing visualisation setup including a monochromatic light source and an adjustable sample using software able to recognise the drop and measure its contact angle. The RTILs are pipetted onto the cleaned substrate stage, adjustable in three dimensions using micrometer screws. The droplet is then centred, and an image is taken for analysis using the software. An averaged contact angle is calculated from the recorded imaging, taking the left and right angles into consideration (within 5% of each other or symmetry).

Figure 3 is an example of the first reported generation of microbubbles in RTILs [60], using fluidic oscillation.

Figure 6

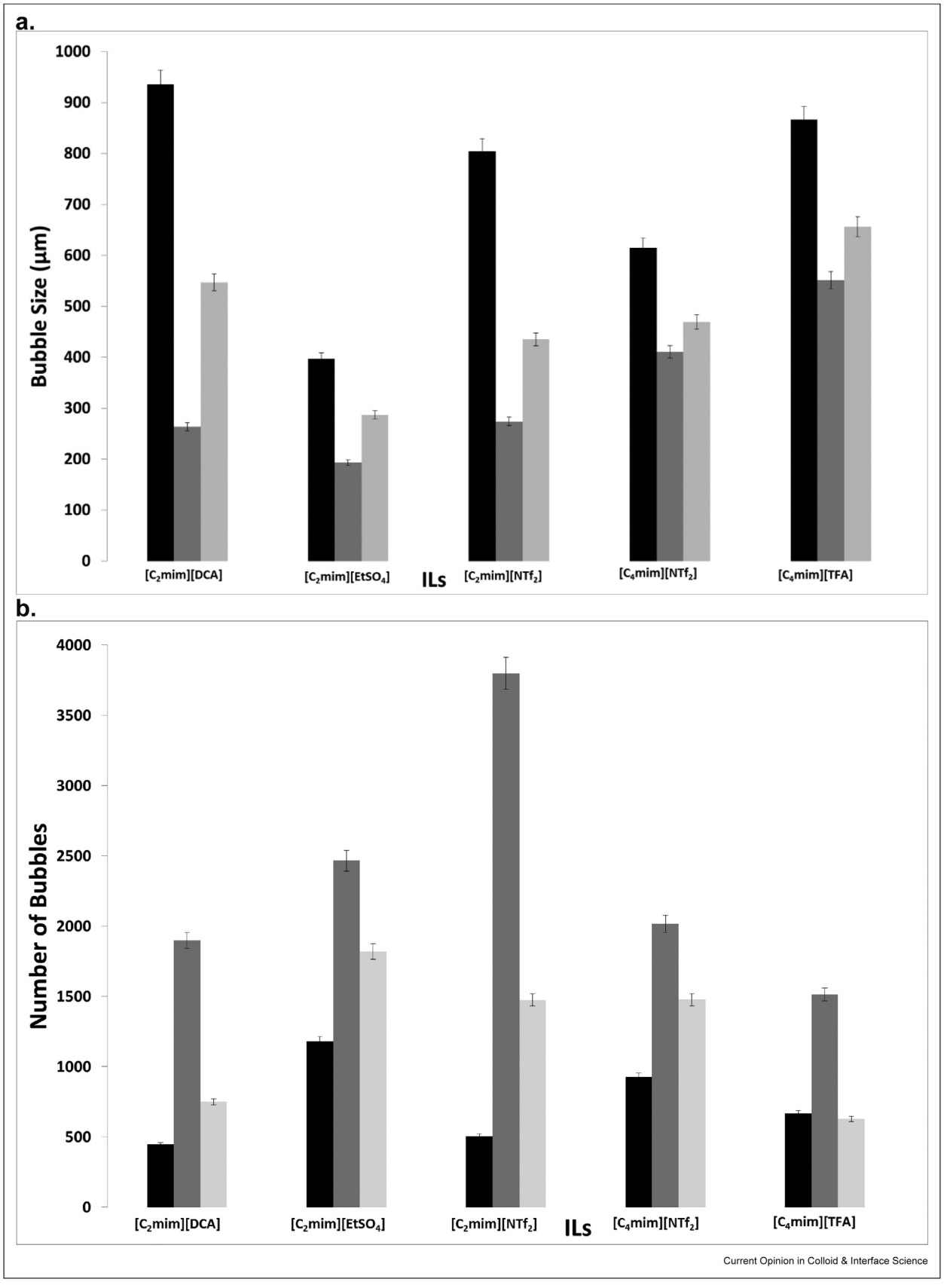
a.
Bubble Size (µm)
1000
900
800
700
600
500
400
300
200
100
0
[C2mim][DCA]
[C2mim][EtSO4]
ILs
[C2mim][NTf2]
[C4mim][NTf2]
[C4mim][TFA]
b.
Number of Bubbles
4000
3500
3000
2500
2000
1500
1000
500
0
[C2mim][DCA]
[C2mim][EtSO4]
[C2mim][NTf2]
ILs
[C4mim][NTf2]
[C4mim][TFA]
Current Opinion in Colloid & Interface Science

Figure 4 shows an example of the BSDs being dominated by the 750- to 800-μm bin for steady flow and the 450- to 500-μm bin for oscillatory flow. It demonstrates the difference in the BSDs at steady flow and oscillatory flow for [C_4mim] [TFA]. The number of bubbles (bubble throughput) is increased significantly for oscillatory flow, which corresponds to the reduced size/volume fraction of the bubble ensemble. The BSD is wide and since larger bubbles are formed; fewer bubbles are formed for the same bubble throughput for conventional steady flow. The BSD is narrower and far more numerous bubbles are formed. The size distribution can be seen to shift to the left for fluidic oscillator—mediated microbubbles in [C_4mim] [TFA].

Figure 5 shows the BSD for conventional steady flow after fluidic oscillator implementation in [C_4mim] [TFA]. This shows a 'morphing' of the two BSDs. The BSDs are merged, with a slight shift to the left compared to the steady flow originally. The smaller bubbles seem to be generated in the size range for when the fluidic oscillator is applied while also produced in the size range where only steady flow had generated the bubbles. This looks like an amalgam of the two conditions, where it is neither steady flow size distribution nor fluidic oscillator flow size distribution but exhibits properties of both the size distributions. As a point of clarification, the steady flow microbubbles and the oscillatory microbubbles both rise within seconds, so that the amalgam of the two distributions is not due to recirculation of the first-stage microbubbles.

This intermediate BSD concurs with the "staging" hypothesis. Figure 6 shows the average bubble size and bubble throughput for the various ILs. The bubble size decreases and correspondingly bubble throughput increases, with fluidic oscillator implementation compared to steady flow. The corresponding bubble size and bubble throughput agrees with the hypothesis for steady flow post fluidic oscillator implementation. The steady flow post fluidic oscillator condition displays a mid-range value of the oscillator and steady flow condition and retains this for a short period of time ($\approx$1600—1800 s). Once the system is flushed/cleaned, this feature is not retained. Desai [60] discusses the role of imbibition and lubrication effects that create the memory/hysteresis effects perceived to explain the staging phenomenon.

The bubble throughput is seen to increase substantially upon fluidic oscillation. The bubble size has reduced by 50% for most cases with [C_2mim][DCA] showing an approximate 3.7-fold reduction in bubble size (940 μm for steady flow down to 260 μm for oscillatory flow) and a 4-fold increase in bubble throughput (from 450 for steady flow up to 1900 for oscillatory flow). Upon subsequent implementation of steady flow post oscillation for [C_2mim][DCA], there is a combination of oscillatory flow and steady flow behaviour observed, which results in a 50% reduction in bubble size (now 547 μm) compared to steady flow or 50% increase in bubble size compared to oscillatory flow and likewise for bubble throughput (now 750). This type of behaviour is observed for all the ILs tested. The interesting behaviour to note is for [C_2mim][NTf_2] where the staging effect observed (steady flow post FO) is closer in size to the steady flow than the FO and can be seen as a direct consequence in the throughput chart. Viscosity and other physico—chemical parameters will be considered next. The important aspects can be seen in the individual BSDs for the three conditions.

Figure 7 shows that steady flow post fluidic oscillation (FO)/steady flow is roughly between 50% and 80% of the steady flow bubble size. This supports the staging effect hypothesis, and this demonstrates how the viscosity and wettability play an integral part in the sizing. When FO/steady flow ratio is plotted, it provides a strong relationship between wetting and bubble size with the viscosity playing a supplementary role in this thereby resulting in reduced bubble size. This is an important conclusion as this is not apparent but agrees well with the hypothesis for the lubrication effect and previous studies [61]. The FO/steady flow post FO demonstrates the 'character' percentage observed for the morphed system and how much the steady flow post FO is compared to the FO. Here, the lower viscosity means that there will be a lower value. Higher the viscosity, higher is this value, which means there is a greater staging observed.

Although the most clear correlation in average bubble-size reduction is with viscosity of the liquid (Figure 7a), increasing contact angle, i.e., decreasing wettability, generally leads to significantly higher percentage reduction in bubble size due to fluidic oscillation, relative to steady flow. However, these two physical properties are not varied independently, so that the major learning is that viscous resistance is more important than wetting in microbubble size reduction. Because the two physical properties are not varied independently, there is no disagreement with the results of Wesley et al. (2016) that show that engineering surface wettability has a strong effect on bubble-size reduction.

Bubble-size distribution (**a**) and throughput (**b**) for the various iconic liquids exhibiting the staging effect observed ■: steady flow, ■: fluidic oscillator, and ■: steady flow post fluidic oscillator implementation.

Figure 7

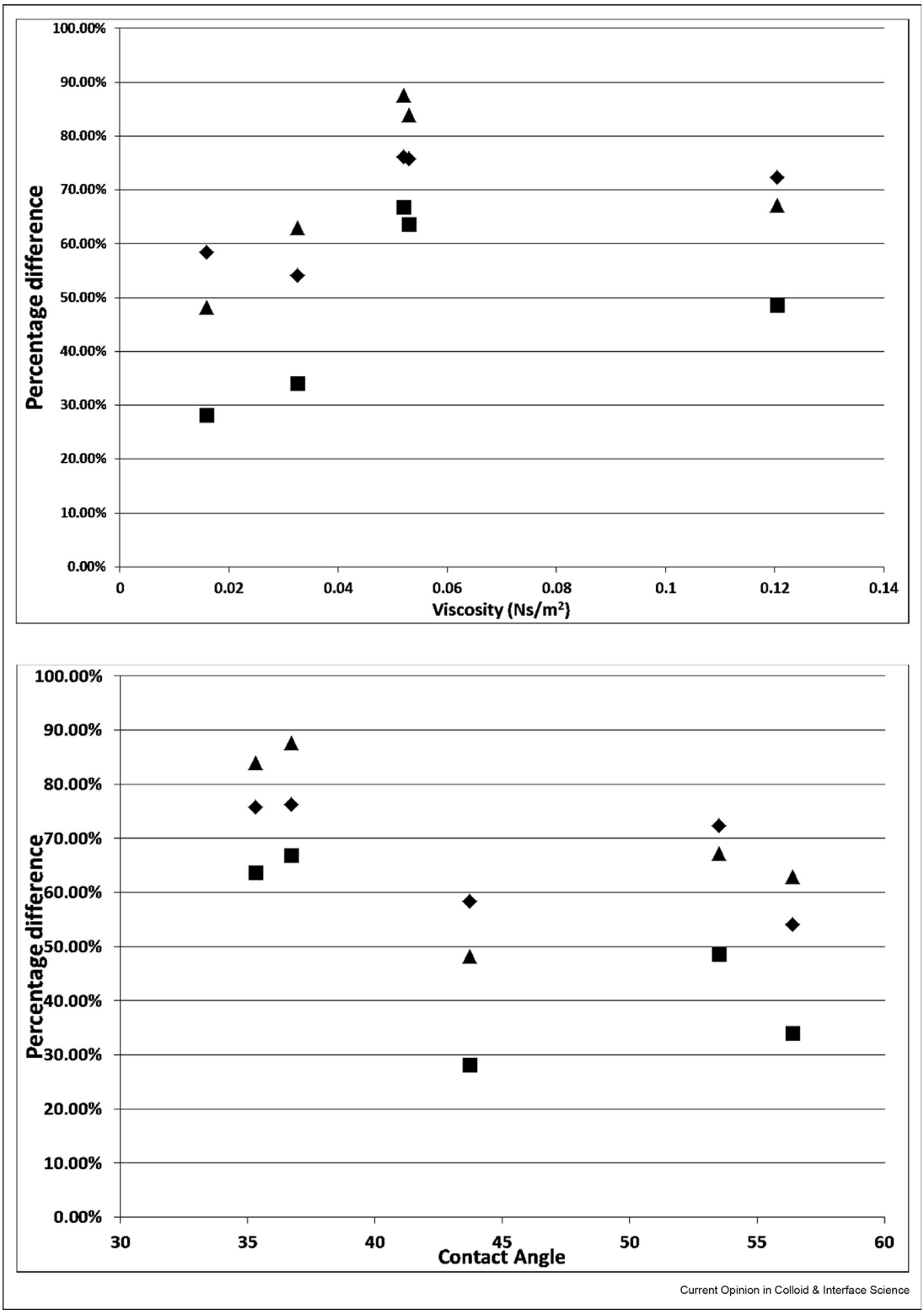

Percentage difference for average bubble sizes at various conditions in various liquids versus their viscosities and contact angle. ◆: $\frac{steady\ flow\ post\ FO}{steady\ flow}$, ■: $\frac{FO}{steady\ flow}$, and ▲: $\frac{FO}{steady\ flow\ post\ FO}$.

Discussion and conclusions

The rationale for this paper was to investigate the extent to which liquid wetting influences microbubble generation, with performance assessed via emergent microbubble-size distribution. Of course, BSDs are inferred in different ways, with comparison being rare and benchmarking to a known standard being almost nonexistent. It should be noted that this investigation has been limited to approaches which produce scalable, dispersed clouds of microbubbles. There is a parallel literature that studies the physics of single microbubble releases, generally with large displacements from other microbubbles, often from a single needle. While these studies of microbubble dynamics in isolation are useful for theoretical understanding, they are very hard to relate to practical applications.

It would be delightful if there were a theoretical guide to wetting effects and microbubble-generation mechanisms. One might imagine that many bubble mechanisms occur with high speed or strong mechanical action, so wetting effects should not be dominant (high capillary and Weber numbers). The counter argument is that high-speed flows have boundary layers, stagnation zones, and stagnation points with complex geometries. So, although surface tension is in the denominator and velocity/squared in the numerator for capillary and Weber numbers, local capillary and Weber numbers in these low-flow zones will self-evidently be small. Nonetheless, the mechanisms for break-up or pinch-off of bubbles are strongly influenced by shear and transient shear, both of which are likely to be dominant in these slow-flow zones. There does not seem to be an agreed standard "wetting–shear" dimensionless group that demonstrably correlates with intensive or extensive BSDs in the literature. Nevertheless, intuitively, the action of these mechanisms must impact the emergent BSD.

This disconnect between scalable approaches for microbubble generation and scientific experiments on microbubble dynamics in isolation is perfectly clear when it comes to exploration of physical properties. Nearly all applications are conducted in aqueous solutions with contaminant chemicals and particulate matter. Nearly all investigations into BSDs are conducted in very clean and clear water (often deionized water), regardless of the generation method.

The line of fundamental physicochemical hydrodynamic scientific investigation of microbubble formation influenced by wetting starts from seminal work of Corchero et al. [64], studying isolated submerged orifices in plates, or the work of Oguz and Prosperetti [65] with bubble growth and detachment from submerged needles. Recent additions to these lines add complexity in constituency. Dousti et al. [66] add nanofluids and study detachment from the needle. Rubio–Rubio et al. [67] show the generation of unexpectedly large bubbles, exceeding the Rayleigh–Taylor instability apparent limit, due to superhydrophobic coatings on the substrate for the isolated aperture. Mirsandi et al. [68] consider the complex hydrodynamic and wetting interaction leading to apparent contact angles/lines as bubbles grow from an orifice in a submerged plate, developing a full two-phase flow model, a local front reconstruction approach that agrees well with the experiments. Sattari and Hanafizadeh [69] study bubble formation from a needle/nozzle, characterising wetting effects, in polymer solutions.

Unfortunately, it is unclear how to generalize these two types of studies when it comes to wetting influence on microbubble cloud dynamics that is scalable—many parallel pores. The difficulty derives from the fundamental fluid dynamical phenomena that lead to maldistribution across many scenarios—the instability of parallel percolation. In porous media flows, the famous viscous fingering instability [70] is an example of this instability. Once a finger nudges ahead of the other proto-fingers, it becomes the path of least resistance. In the case of an array of micropores, feed from the same gas-filled chamber, submerged in liquid, the largest bubble that forms then provides the path of least resistance, preferentially growing against all other bubbles in the parallel percolation process in a nozzle bank or porous ceramic material [71].

The consequence of this phenomenon is that studying single bubble formation dynamics from an orifice or needle is not representative of the generation dynamics of a whole cloud, nor the interaction dynamics of a cloud of microbubbles once dispersed. The scientific approach is typically to idealize an experiment so that the target phenomenon is studied in isolation, from which complexity is successively added. Unfortunately, some phenomena have irreducible complexity. The most one can hope for in such scenarios is to focus on a microcosm within the complex system. Since in this article we have found several exemplar works that demonstrate the significant influence of wetting on several classes of industrially scalable microbubble generation, while arguing for the deduction that wetting is important in all five classes explored here, it is our hope that fundamental experimental scientists turn their attention to characterisation of the physicochemical hydrodynamics of the scalable classes of microbubble generation. The diagnostics for whole-cloud characterisation of dispersed microbubbles are reviewed here, but those approaches deployed for single microbubbles have ready applications to focus on the microcosm within the complex system. In particular, wetting effects studies such as Li et al. [55] within the venturi for hydrodynamic cavitation are recommended for within DAF nozzles and rotary pump mixers for microbubble generation.

Declaration of competing interest

The second author is a shareholder in Perlemax Ltd. for which the first author is the CEO. However, the work reported in this paper was conducted prior to that appointment during the doctoral studies of the principal author.

Data availability

No data was used for the research described in the article.

Acknowledgments

The authors acknowledge gratefully the Engineering and Physical Sciences Research Council for supporting this work financially (Grant nos. EP/N011511/1, EP/P030238/1, EP/K001329/1, EP/I019790/1). InnovateUK, IIKE, The Royal Society, AECOM Design Build, and Viridor are acknowledged for funding support. The many colleagues who have contributed discussions and technical support leading to the insights in this paper, including M. Al-Mashhadani, H. Bandulasena, V. Tesar, G.Greenwood, H.Mohammed, SR Taylor, C. Hardacre, J. Jacquemin, R. Allen, S.Brittle, L.Tse, W.Zhou, P.Verrier,E.Baril, W. Nugroho, Y.Sharma, G.Yadav, U. Haji Hassan, M du Prees Thomas, E. Akototse, H.Khudair, B. Franklin, A. Dunbar,G. Medley, M. Hines, J. Pandhal, H. Jensen, DJ Gilmour S. Vaidyanathan, are thanked for their assistance.

References

Papers of particular interest, published within the period of review, have been highlighted as:

* * of outstanding interest

1. Agarwal A: **Principle and applications of microbubble and nanobubble technology for water treatment**. *Chemosphere* 2011, **84**:1175–1180.

2. Fujiwara A, Okamoto K, Hashiguchi K, Peixinho J, Takagi S, Matsumoto Y: **Bubble breakup phenomena in a venturi tube**. July 30–August 2 *ASME Fluids Engineering Division Summer Meeting* 2007, https://doi.org/10.1115/FEDSM2007-37243. San Diego, California, USA.

3. Ranade VV, Bhandari VM, Nagarajan S, Sarvothaman VP, Simpson AT: *Hydrodynamic cavitation: devices, design, and application*. Weinheim, Germany: Wiley VCH; 2023.

4. Takahashi M: **Base and technological application of microbubble and nanobubble**. *Mater Int* 2009, **22**:2–19.

5. Desai PD, Zimmerman WB: **Microbubble Intensification of Bioprocessing: The role of direct microorganism and bubble interactions**. *J.Mat. Tech. Rev.* 2023, **67**, https://doi.org/10.1595/205651323X16778518231554.

6. Krzan M, Chattopadhyay P, Orvalho S, Zednikova M: **Effects of N-alkanol adsorption on bubble acceleration and local velocities in solutions of the homologous series from ethanol to N-decanol**. *Materials* 2023, **16**:2125, https://doi.org/10.3390/ma16052125.

7. Singhal S, Moser CC, Wheatley MA: **Surfactant-stabilized microbubbles as ultrasound contrast agents: stability study of Span 60 and Tween 80 mixtures using a Langmuir trough**. *Langmuir* 1993, **9**:2426–2429, https://doi.org/10.1021/la00033a027.

8. Patel R, Lacerda W, Oeffinger BE, Eisenbre JR, Rochani AK, Kaushal G, Wessner CE, Wheatley MA: **Development of a dual drug-loaded, surfactant-stabilized contrast agent containing oxygen**. *Polymers* 2022, **14**:1568, https://doi.org/10.3390/polym14081568.

9. Edzwald JK: **Dissolved air flotation and me**. *Water Res* 2010, **44**:2077–2106.

10. Desai P, Ng W, Hines M, Riaz Y, Tesar V, Zimmerman W: **Comparison of bubble size distributions inferred from acoustic, optical visualisation, and laser diffraction**. *Colloids and Interfaces* 2019, **3**:65.

11. Wesley DJ, Brittle SA, Toolan DTW, Howse JR, Zimmerman W: **Development of an optical microscopy system for automated bubble cloud analysis**. *Appl Opt* 2016, **55**:6102–6107.

12. Schmideder S, Thurin L, Kaur G, Briesen H: **Inline imaging reveals evolution of the size distribution and the concentration of microbubbles in dissolved air flotation**. *Water Res* 2022, **224**:119027.

13. Le NNH, Sugai Y, Nguele R, Sreu T: **Bubble size distribution and stability of CO2 microbubbles for enhanced oil recovery: effect of polymer, surfactant and salt concentrations**. *J Dispersion Sci Technol* 2021, https://doi.org/10.1080/01932691.2021.1974873.

14. Yan G, Cheng Z, Ma Y, Scheuermann A, Li L: **Applying imaging technique to investigate effects of solute concentrations and gas injection rates on gas bubble generation**. *Geofluids* 2022: 2046267.

15. Yoo Y, Ga S, Kim J, Cho H: **Method for measuring bubble size under low-light conditions for mass transfer enhancement in industrial-scale systems**. *Int Commun Heat Mass Tran* 2023, **140**:106525.

16. **Experimental diagnostics in gas-phase combustion systems: AIAA progress in astronautics and aeronautics**Swithenbank J, Beer J, Taylor DS, Abbott D, McCreath CO, Zinn BT. *AIAA* 1977, **53**:421.

17. Couto HJB, Nunes DG, Neumann R, França SCA: **Micro-bubble size distribution measurements by laser diffraction technique**. *Miner Eng* 2009, **22**:330–335.

18. Wang Y, Thanyamanta W, Bulger C, Bose N: **Experimental study to make gas bubbles as proxies for oil droplets to test AUV detection of oil plumes**. *Appl Ocean Res* 2022, **121**:103080.

19. Gao Y, Dashliborun AM, Zhou JZ, Zhang X: **Formation and stability of cavitation microbubbles in process water from the oilsands industry**. *Ind Eng Chem Res* 2021, **60**:3198–3209.

20. Leighton TG: *The acoustic bubble*. Cambridge, MA, USA: Academic Press; 1994.

21. Friedrichs KO, Keller JB: **Geometrical acoustics. II. Diffraction, reflection, and refraction of a weak spherical or cylindrical shock at a plane interface**. *J Appl Phys* 1955, **26**:961.

22. Wu X, Chahine GL: **Development of an acoustic instrument for bubble size distribution measurement**. *J Hydrodyn* 2010, **22**: 325–331.

23. Wu X, Hsiao C-T, Choi J-K, Chahine GL: *Measurement of bubble size distribution based on acoustic propagation in bubbly medium*. Baltimore, MD: APS March Meeting; 2013:18–22. May.

24. Wu X, Wendel H, Chahine GL, Reimer B: **Gas bubble size measurements in liquid mercury using an acoustic spectrometer**. *J Fluid Eng* 2014, **136**:31303. 1.

25. Nye AL, Wu X, Chahine GL: *Bubble generation and sizing in fresh and salt water*. Baltimore, MD: International Conference on Two-Phase Systems for Ground and Space Applications; 2014, https://doi.org/10.13140/2.1.3972.6406.

26. Shin M-S, Moon I-S, Nah Y-I, Park J-C: **Bubble wake measurement by acoustic bubble spectrometer generated by planing hull at circulating water channel**. *Journal of the Korea Institute of Military Science and Technology* 2011, **14**, https://doi.org/10.9766/KIMST.2011.14.1.055.

27. Desai PD, Hines MJ, Riaz Y, Zimmerman WB: **Resonant pulsing frequency effect for much smaller bubble formation with fluidic oscillation**. *Energies* 2018, **11**:2680, https://doi.org/10.3390/en11102680.

28. Chen X, Hussein M, Becker T: **Determination of bubble size distribution in gas–liquid two-phase systems via an ultrasound-based method**. *Eng Life Sci* 2017, **17**:653–663.

29. Wesley DJ, Smith RM, Howse JR, Zimmerman WB: **The influence of surface wettability on microbubble formation**. *Langmuir* 2016, **32**:1269–1278.

30. Krasowska M, Malysa K, Beattie DA: **Recent advances in studies of bubble-solid interactions and wetting film stability**. *Curr Opin Colloid Interface Sci* 2019, **44**:48–58.

31. Wang H, Zhang Y, Wang C: **Surface modification and selective flotation of wasteplastics for effective recycling – a review**. *Separ Purif Technol* 2019, **226**:75–94.

32. Sadeghi M, Hashem Ri, Shahverdi H: **A contribution to flotation technique as a reliable wettability alteration measurement method for carbonate minerals in separation processes involving hydrocarbons, low salinity water and nanofluids**. *Colloids Surf A Physicochem Eng Asp* 2022, **633**:127912.

33. Liu B, Manica R, Xu Z, Liu Q: **The boundary condition at the air–liquid interface and its effect on film drainage between colliding bubbles**. *Curr Opin Colloid Interface Sci* 2020, **50**: 101374.

34. Vakarelski IU, Yang F, Thoroddsen ST: **Effects of interface mobility on the dynamics of colliding bubbles**. *Curr Opin Colloid Interface Sci* 2022, **57**:101540.

35. Chen A, Yang W, Geng S, Gao F, He T, Wang Z, Huang Q: **Modeling of microbubble flow and coalescence behavior in the contact zone of a dissolved air flotation tank using a computational fluid Dynamics–Population balance model**. *Ind Eng Chem Res* 2019, **58**:16989–17000.

36. Yang M, Fernandes del Pozo D, Torfs E, Rehman U, Yu D, Nopens I: **Numerical simulation on the effects of bubble size and internal structure on flow behavior in a DAF tank: a comparative study of CFD and CFD-PBM approach**. *Chemical Engineering Journal Advances* 2021, **7**:100131.

37. Sadatomi M, Kawahara A, Kano K, Ohtomo A: **Performance of a new microbubble generator with a spherical body in a flowing water tube**. *Exp Therm Fluid Sci* 2005, **29**:615–623.

38. Regunath GS, Zimmerman WB, Tesar V, Hewakandamby BN: **Experimental investigation of helicity in turbulent swirling jet using dual plane dye laser technique**. *Exp Fluid* 2008, **45**.

39. Zimmerman WB: **Fluctuations in concentration due to convection by a helical flow in a conducting fluid**. *Phys Fluid* 1996, **8**:1631–1642.

40. ** Wang X, Shuaia Y, Zhoua X, Huanga Z, Yanga Y, Suna J, Zhang H, Wang J, Yang Y: **Performance comparison of swirl-venturi bubble generator and conventional venturi bubble generator**. *Chem Eng Process: Process Intensif* 2020, **154**:108022.
Swirling flow is an excellent way to condition turbulence to achieve localized regions of high-helicity intensity. This is important for introducing handedness to microbubble dynamics, hence influencing chirality of chemical interaction on microbubble interfaces.

41. ** Murai Y, Tasaka Y, Oishi Y, Ern P: **Bubble fragmentation dynamics in a subsonic Venturi tube for the design of a compact microbubble generator**. *Int J Multiphas Flow* 2021, **139**:103645.
For a long time, venturi tubes were thought to be unable to generate microbubbles smaller than 100 microns in diameter on average. The fragmentation-dynamics mechanism exploited here in strong shear flows induced by the geometric configuration design are potentially a godsend to this approach.

42. Kim D, Jang Gil Kim JG, Chu CN: **Aging effect on the wettability of stainless steel**. *Mater Lett* 2016, **170**:18–20.

43. Li M, Bussonnière A, Bronson M, Xu Z, Liu Q: **Study of Venturi tube geometry on the hydrodynamic cavitation for the generation of microbubbles**. *Miner Eng* 2019, **132**:268–274.

44. ** Simpson A, Ranade VV: **Modeling hydrodynamic cavitation in venturi: influence of venturi configuration on inception and extent of cavitation**. *AIChE J* 2019, **65**:421–433.
Theoretical underpinnings of the experimental work of Li et al. (2022) showing that wetting can indeed influence cavitation in venturi tubes.

45. ** Liu G, Bie H, Hao Z, Wang Y, Ren W, Hua Z: **Characteristics of cavitation onset and development in a self-excited fluidic oscillator**. *Ultrason Sonochem* 2022, **86**:106018.
Fluidic oscillators that achieve either high frequency or very sharp switching have inherently high local pressure gradients, as well as reverse flow, so they can induce strong rarefaction effects that are a precursor to cavitation bubble formation.

46. Tesař V: **Taxonomic trees of fluidic oscillators**. *EPJ Web Conf. EFM16 – Experimental Fluid Mechanics* 2017, **143**:2128.

47. Swart B, Pihlajamaki A, John Chew JM, Wenk J: **Microbubble-microplastic interactions in batch air flotation**. *Chem Eng J* 2022, **449**:137866.

48. Li P, Tsuge H: **Water treatment by induced air flotation using microbubbles**. *J. Chem. Eng. Soc. Japan* 2006, **39**:896–903.

49. Song Chung MM, Tsai J-H, Lu J, Padilla Chevez M, Huang J-Y: **Microbubble-assisted cleaning to enhance the removal of milk deposits from the heat transfer surface**. *ACS Sustainable Chem Eng* 2022, **10**:8380–8387.

50. Sheng Y, Zhang X, Zhai X, Zhang F, Li G, Zhang D: **A mobile, modular and rapidly-acting treatment system for optimizing and improving the removal of non-aqueous phase liquids (NAPLs) in groundwater**. *J Hazard Mater* 2018, **360**:639–650.

51. Gilmour DJ, Zimmerman WB: **Microbubble intensification of bioprocessing**. *Adv Microb Physiol* 2020, **77**:1–35.

52. Swart B, Zhao Y, Khaku M, Che E, Maltby R, John Chew JM, Wenk J: ***In situ* characterisation of size distribution and rise velocity of microbubbles by high-speed photography**. *Chem Eng Sci* 2020, **225**:115836.

53. Alfarraj BA, Alkhedhair AM, Al-Harbi AA, Nowak W, Alfaleh SA: **Measurement of the air bubble size and velocity from micro air bubble generation (MBG) in diesel using optical methods**. *Energy Transitions* 2020, **4**:155–162.

54. Leighton TG: **What is ultrasound**. *Prog Biophys Mol Biol* 2007, **93**:3–83.

55. ** Li M, Bussonnière A, Xiang B, Manica R, Liu Q: **Effect of solid wettability on three-phase hydrodynamic cavitation**. *Miner Eng* 2022, **180**:107455.
One of the three main exemplars of wettability effects on formation of microbubbles, and therefore, an encouragement to all classes of microbubble generators to consider not just hydrodynamics on microbubble generation, but how surface coatings that change wettability influence microbubble performance?

56. Al-Mashhadani MKH, Bandulasena HCH, Zimmerman WB: **CO_2 mass transfer induced through an airlift loop by a microbubble cloud generated by fluidic oscillation**. *Ind Eng Chem Res* 2012, **51**:1864–1877.

57. Song A, Zhao S, Cao Y, Li C: **Effect of sparger characteristics on bubble-formation dynamics under oscillatory air pattern**. *Processes* 2022, **10**:997.

58. Tesař V: **Fluidic generator of microbubbles – oscillator with gas flow reversal for a part of period**. *Acta Mech Automatica* 2015, **9**:195–203.

59. Xie B, Zhou C, Huang X, Chen J, Ma X, Zhang J: **Microbubble generation in organic solvents by porous membranes with different membrane wettabilities**. *Ind Eng Chem Res* 2021, **60**: 8579–8587.

60. ** Desai PD: *A fluidic oscillator based on a new mechanism: for microbubble generation and developing microbubble stripping for separation phenomena*. PhD thesis. University of Sheffield; 2018.
Introduced a new fluidic oscillator with nearly monochromatic pressure-wave spectrum downstream of the resonators—decreases friction losses and dispersion losses for microbubble generation with the strongest pulse yet achieved for a given pressure drop across an oscillator.

61. Taylor SFR, Brittle SA, Desai P, Jacquemin J, Hardacre C, Zimmerman WB: **Factors affecting bubble size in ionic liquids**. *Phys Chem Chem Phys* 2017, **19**:14306–14318.

62. Holbrey JD, Reichert WM, Swatloski RP, Broker GA, Pitner WR, Seddon KR, Rogers RD: **Efficient, halide free synthesis of new, low cost ionic liquids: 1,3-dialkylimidazolium salts containing methyl- and ethyl-sulfate anions**. *Green Chem* 2002, **4**: 407–413.

63. Lu W, Ma J, Hu J, Song J, Zhang Z, Yang G, Han B: **Efficient synthesis of quinazoline-2,4(1*H*,3*H*)-diones from CO2 using ionic liquids as a dual solvent–catalyst at atmospheric pressure**. *Green Chem* 2014, **16**:221–225.

64. Corchero G, Medina A, Higuera FJ: **Effect of wetting conditions and flow rate on bubble formation at orifices submerged in water**. *Colloids Surf A Physicochem Eng Asp* 2006, **290**:41–49.

65. Oguz HN, Prosperetti A: **Dynamics of bubble growth and detachment from a needle**. *J Fluid Mech* 1993, **257**:111–145.

66. Dousti A, Gharedaghi H, Hanafizadeh P, Ashjaee M: **Different nanofluids effect on bubble characteristics at the isothermal bubble column**. *Can J Chem Eng* 2021, **99**:S901–S914.

67. Rubio-Rubio M, Bolaños-Jiménez R, Martínez-Bazán C, Muñoz-Hervás JC, Sevilla A: **Superhydrophobic substrates allow the generation of giant quasi-static bubbles**. *J Fluid Mech* 2021, **912**:A25.

68. Mirsandi H, Smit WJ, Kong G, Baltussen WM, Peters EAJF, Kuipers JAM: **Influence of wetting conditions on bubble formation from a submerged orifice**. *Exp Fluid* 2020, **61**:83.

69. Sattari A, Hanafizadeh P: **Bubble formation on submerged micrometer-sized nozzles in polymer solutions: an experimental investigation**. *Colloids Surf A Physicochem Eng Asp* 2019, **564**:10–22.

70. Zimmerman WB, Homsy GM: **Nonlinear viscous fingering in miscible displacement with anisotropic dispersion**. *Phys Fluid* 1991, **3**:1859.

71. Zimmerman WB, Hewakandamby BN, Tesař V, Bandulasena HCH, Omotowa OA: **On the design and simulation of an airlift loop bioreactor with microbubble generation by fluidic oscillation**. *Food Bioprod Process* 2009, **87**: 215–227.

72. Tsuge H: *Micro-and nanobubbles fundamentals and applications*. Pan Stanford; 2014.